Initial GPS scintillation results from CASES receiver at South Pole, Antarctica

K. B. Deshpande,[1] G. S. Bust,[2,3] C. R. Clauer,[1] H. Kim,[1] J. E. Macon,[1] T. E. Humphreys,[4] J. A. Bhatti,[4] S. B. Musko,[5] G. Crowley,[2] and A. T. Weatherwax[6]

Received 3 June 2012; revised 7 September 2012; accepted 17 September 2012; published 31 October 2012.

[1] Connected Autonomous Space Environment Sensor (CASES) Global Positioning System (GPS) software-defined receivers developed for ionospheric scintillation studies have been deployed on Autonomous Adaptive Low-Power Instrument Platforms (AAL-PIP) at South Pole, Antarctica. In this paper, we describe the AAL-PIP experimental setup focusing on CASES. We explain in detail the method developed for analyzing CASES data, and report initial AAL-PIP CASES results. Furthermore, we compare the CASES measurements with those from a modified Novatel GSV4004 GPS Ionospheric Scintillations and TEC Monitor (GISTM) receiver at the South Pole. CASES receivers have been successfully deployed and reliably operated in equatorial and midlatitude regions. Four of these GPS receivers, for the first time, are deployed in high-latitude regions as a part of the National Science Foundation (NSF) funded project of deploying space science instrument platforms, AAL-PIPs, in Antarctica since December 2010–2011. We present initial scintillation results recorded by a CASES receiver at South Pole during the storm on 24 January 2012 along with AAL-PIP magnetometer observations. We have deduced that the CASES receiver scintillation observations agree with those from the Novatel GPS scintillation receiver. Since this is the first time a CASES receiver has been deployed to operate in a high latitude, low temperature, and low humidity environment, we consider this comparison a demonstration of its reliable operation as a science-grade scintillation receiver in such conditions. We plan to study high latitude ionospheric irregularities by using observations from CASES and other ancillary instruments from Antarctica coupled with physical parameters derived from models.

Citation: Deshpande, K. B., G. S. Bust, C. R. Clauer, H. Kim, J. E. Macon, T. E. Humphreys, J. A. Bhatti, S. B. Musko, G. Crowley, and A. T. Weatherwax (2012), Initial GPS scintillation results from CASES receiver at South Pole, Antarctica, *Radio Sci.*, *47*, RS5009, doi:10.1029/2012RS005061.

1. Introduction

[2] Ionospheric irregularities caused by electron density fluctuations in the ionosphere disturb a traversing radio signal leading to distortion of its phase and amplitude. These signal distortions, as observed from the ground, are known as ionospheric scintillations. Detailed information on the relationship between ionospheric irregularities and scintillations can be found in the work of *Wernik et al.* [2003]. Scintillations are frequently observed in high latitude and equatorial regions. As summarized by *Aarons* [1982], the occurrence of scintillations is also dependent on the phase of the solar cycle, the season, and the time of the day. Global Positioning System (GPS) signals can suffer fading, and GPS receivers may even lose lock on the signal due to ionospheric scintillation. However, if these scintillation-induced GPS signal phase and amplitude variations are regarded as valuable scientific data instead of nuisance, then the nearly worldwide availability of GPS signals can be utilized for studies of scintillations at high latitudes. Considering the historic inaccessibility of these regions, such studies could prove extremely useful.

[3] Much prior research has exploited GPS as a tool for studying scintillations. *Akos et al.* [2001] and *Ganguly et al.* [2004] present different software-based approaches for implementing a GPS ionospheric monitoring receiver.

[1]Bradley Department of Electrical and Computer Engineering, Virginia Polytechnic Institute and State University, Blacksburg, Virginia, USA.
[2]Atmospheric and Space Technology Research Associates, Boulder, Colorado, USA.
[3]Now at The Johns Hopkins University Applied Physics Laboratory, Laurel, Maryland, USA.
[4]Aerospace Engineering and Engineering Mechanics, University of Texas at Austin, Austin, Texas, USA.
[5]Department of Atmospheric, Oceanic and Space Sciences, University of Michigan, Ann Arbor, Michigan, USA.
[6]Department of Physics, Siena College, Loudonville, New York, USA.

Corresponding author: K. B. Deshpande, Center for Space Science and Engineering Research, Bradley Department of Electrical and Computer Engineering, Virginia Polytechnic Institute and State University, Space@VT, 1901 Innovation Dr., Suite 1000 MC0549, Blacksburg, VA 24061, USA. (kshitija@vt.edu)

0048-6604/12/2012RS005061

Furthermore, *Skone et al.* [2005] offer test results for a GPS software receiver in simulated high-latitude scintillation conditions. As *Beach* [1982] and *Basu et al.* [2002] indicate, equatorial ionospheric irregularities display ordered motion, are field-aligned, and have been studied in detail for several years with an abundant number of GPS scintillation monitoring receivers deployed in the near-equator regions. *Basu et al.* [2002] imply that high latitude irregularities produce short-lived GPS scintillations, making the former more challenging to characterize. Moreover, solar wind and magnetospheric plasmas are connected to the auroral regions of the ionosphere through complex magnetosphere-ionosphere coupling mechanisms. High latitude irregularities are, therefore, a result of different systems interacting with each other. GPS scintillation measurements combined with physical parameters such as width, height, drift speed of the irregularities, and other values derived from modeling can be used to study the physical properties of ionospheric irregularities. *Coster et al.* [2005] reviewed characteristics of scintillations in the auroral and polar cap regions and their relationship with storm enhanced density (SED) by using GPS total electron content (TEC) mapping. Additionally, diffractive fading of GPS signals has been observed by *Smith et al.* [2008] in the auroral region as a consequence of E-region precipitation. High latitude GPS scintillations have been reported in the northern polar regions over a few years [*Skone and Knudsen*, 2000; *Mitchell et al.*, 2005; *Spogli et al.*, 2009; *Prikryl et al.*, 2010].

[4] The southern high latitudes have been inaccessible for several years mostly due to the lack of infrastructure and the harsh environment in Antarctica. Advances in the cold weather operations in Antarctica as well as state-of-the-art power system technology have allowed the deployment of autonomous GPS scintillation receivers in remote regions. Some recent GPS scintillation studies by *Ngwira et al.* [2010], *Prikryl et al.* [2011] and *Kinrade et al.* [2012] from Antarctica display promise for the high latitude GPS studies from the southern polar and auroral regions.

[5] In this paper, a geomagnetic storm on 24 January 2012 is studied as a means to evaluate the performance of a new, custom-designed, relatively inexpensive Connected Autonomous Space Environment Sensor (CASES) GPS scintillation monitoring receiver in Antarctica. This is the first time a CASES receiver has been used at high latitudes. In section 2, we describe our experimental setup, including a description of the CASES instrument. A data analysis procedure developed for analyzing scintillation data from the CASES receiver is described in section 3. Storm day results from the CASES receiver on System 4, one of the Autonomous Adaptive Low-Power Instrument Platforms (AAL-PIP), which is deployed at the South Pole for testing purposes for a year, are described in section 4. In the same section, we validate our results by comparing them with scintillation data from a modified Novatel GSV4004 GPS Ionospheric Scintillations and TEC Monitor (GISTM) receiver deployed at the South Pole and maintained by the University of Bath, UK and the British Antarctic Survey (BAS).

2. Experimental Setup

[6] As a part of collaborative efforts to understand the space environment of the Earth and its global dynamical response to external and internal influences, a Polar Experiment Network for Geospace Upper-atmosphere Investigations (PENGUIn) team has been established. The PENGUIn AAL-PIP project under National Science Foundation (NSF) support calls for deployment of a chain of six AAL-PIPs, four of which support fluxgate and induction magnetometers as well as dual frequency CASES GPS receivers. The other two stations are of an earlier design and support only fluxgate magnetometers.

[7] The array of AAL-PIP Antarctic stations will boast a handful of cutting-edge technological advances designed to optimize data collection and power management for year-round sustained operation. As described by *Musko et al.* [2009], a major focus of the original system development was to build a low-power platform with a single fluxgate magnetometer specifically designed to operate autonomously in remote Antarctic regions. The platform has now been upgraded to support three instruments: a fluxgate magnetometer, a searchcoil magnetometer, and CASES. The upgraded platforms are capable of unattended operation for at least three years at temperatures as low as -80° Celsius and near real-time data retrieval via satellite communications.

[8] An AAL-PIP utilizes solar energy and stores power in sealed lead-acid batteries for winter operation. The AAL-PIP power system consists of six 40 W solar panels and 16 lead-acid batteries. A super-insulated electronics box supports power control, communication electronics, and data management for all three instruments. The temperature inside the electronics box is maintained at -28° Celsius throughout the winter.

[9] CASES, originally developed to be paperback-novel sized, was customized to a cubic form factor (10 cm $\times$ 10 cm $\times$ 10 cm) to fit inside the compact electronics box of AAL-PIP. Furthermore, during the development, the receiver passed the cold soak test below -50° Celsius and demonstrated reliable operation at about -40° Celsius before and after the test. CASES receivers on the AAL-PIP systems are connected to Antcom GPS antennas.

[10] The CASES receiver is a scientific grade, low-cost, dual-frequency GPS receiver developed by Cornell, UT Austin, and Atmospheric & Space Technology Research Associates (ASTRA). *Crowley et al.* [2011] and *O'Hanlon et al.* [2011] describe the development of CASES, its specifications, characteristics, and operation in detail. All the data acquisition and tracking operations as well as science and navigation related operations, such as TEC computations, scintillation monitoring, and calculation of navigation solution and GPS observables, are performed on a general purpose digital signal processor (DSP). Based on real-time data processing by a scintillation monitor called "SCINTMON," the DSP outputs low-rate scintillation data at up to 10 Hz and high-rate data at up to 100 Hz. The data are then routed to a single board computer that runs a server program for data logging and remote monitoring. As an ionospheric scintillation monitor, CASES has many advantages as described by *Crowley et al.* [2011], including GPS L2 civil code (L2C) tracking capability, incorporation of specialized tracking loops designed for operation in both weak-signal and scintillating environments, and connectivity via a number of different options. CASES on AAL-PIPs may be accessed through an Iridium link for remote logging, reconfiguration and reprogramming.

[11] CASES employs a temperature-compensated crystal-oscillator (TCXO) as its reference oscillator. As *Van Dierendonck et al.* [1993] point out, phase variations caused by TCXO instability manifest a significant spectral overlap with those induced by ionospheric scintillation. It is imperative, therefore, to isolate and remove these clock effects to avoid false detection of phase scintillation. As suggested by *Van Dierendonck et al.* [1993], receiver clock errors can be removed by subtracting a non-scintillating "reference" channel from a scintillating channel. In the unlikely scenario that all channels are scintillating, the reference channel is chosen to be one of two channels with the lowest scintillation power ratio, a metric defined in the work of *O'Hanlon et al.* [2011]. Once these clock effects are removed, SCINTMON operates on the clock-free phase time history and complex accumulations to estimate scintillation of interest.

[12] At high latitudes, phase scintillations are observed more often than amplitude scintillations. A study on the distribution and dynamics of irregularities in the dayside auroral region by *Basu et al.* [1998] indicated large-scale phase variations without the presence of amplitude scintillations. More recent observations reported by *Mitchell et al.* [2005] in northern high latitudes and *Kinrade et al.* [2012] in southern high latitudes also showed a predominance of phase scintillations. To ensure triggering sensitivity to both phase and amplitude scintillation, CASES implements a novel triggering strategy, whose detection statistic is based on the power spectrum of complex (in-phase and quadrature) accumulations. The triggering strategy, first described by *O'Hanlon et al.* [2011], has been shown to be a reliable indicator of scintillation when tested on historical scintillation data from both low and high latitude regions.

[13] CASES implements data capture and retrieval as follows. To prevent loss of interesting scintillation data, CASES temporarily collects high-rate data on a variable-length circular buffer (a 120-second buffer was used to obtain the empirical results reported in this paper). SCINTMON processes these data in real-time in batch intervals (typically 100 seconds) and implements the scintillation triggering algorithm. A trigger indicates the presence of a phase or amplitude fluctuation more vigorous than the user-specified triggering threshold. In response to a triggering event, CASES outputs the contents of the circular buffer, thereby ensuring that a complete picture of the scintillation event is captured, including the quiet prelude before the onset of scintillation. High-rate data are recorded typically at 50 Hz as raw complex accumulations and beat carrier phase. As mentioned earlier, the communication with each remote AAL-PIP is provided by an Iridium link. With a daily upload-download limit of 16 MB, data collected by all three space science instruments on board, namely, the fluxgate magnetometer, the search-coil magnetometer and the CASES GPS receiver, need to be constrained. Each of the magnetometers collects about 1 MB of data per day. Thus, in normal daily operation, CASES collects low-rate data and triggered high-rate data until the daily memory limit for GPS data collection of about 12 to 13 MB is reached. Its scintillation triggering strategy enables CASES to make maximal use ofits allotted daily data limit by capturing and passing along high-rate data only spanning the most vigorous scintillation events. Moreover, a special AAL-PIP "storm mode" can be enabled in anticipation of an incoming solar storm. In storm mode, CASES is allowed to store much more than the standard daily data limit. Data stored locally in storm mode are retrieved over a period of several days post-storm. Data presented in this paper were collected in storm mode.

3. Data Processing

[14] In scintillation studies, two scintillation parameters, viz., scintillation index $S4$ and standard deviation of detrended phase σ_ϕ, are commonly used to indicate the occurrence of amplitude and phase scintillations, respectively. These parameters are computed from detrended high-rate power and phase data. Analysis of single-frequency GPS data for ionospheric scintillation studies requires removing low frequency systematic effects such as those from the troposphere, satellite geometry, and the receiver oscillator. Post-processing involved in the analysis of CASES single frequency high-rate data is elaborated in this section.

[15] As described in section 2, CASES continuously collects low-rate processed data, but only collects high-rate carrier phase and IQ data (typically at 50 Hz) when the scintillation trigger detects an interesting event. The receiver outputs low-rate and high-rate data in the form of binary files that can be converted into ASCII text files called *scint.log* and *iq.log*, respectively. As mentioned earlier, the receiver clock errors introduced into the phase data by the CASES TCXO may generate phase fluctuations that appear similar to phase scintillations. These errors can be eliminated by a simple operation of subtracting carrier and IQ phase of a non-scintillating reference channel from those of a possibly scintillating channel. The IQ phase is defined in terms of the in-phase and quadrature phase components as $\arctan(Q/I)$. In this description, a continuous stream of data from a single GPS satellite identified by its pseudo random noise (PRN) number is referred to as a channel. We have adapted a simple method of reading and processing high-rate data for the clock error removal. For each PRN, we accumulate the available high-rate data from the *iq.log* file and determine the reference channels from the *scint.log* file at times corresponding to these data. Following this examination, we construct data segments of continuous carrier phase of scintillating PRNs at times coinciding with those of the high-rate carrier phase for reference PRNs. We subsequently subtract the reference PRN phase data from the scintillating PRN phase data to obtain differenced carrier phase, free of receiver clock error.

[16] Elimination of clock error is followed by removal of satellite geometry effects. We use a method of polynomial fit subtraction on the continuous segments of data to remove most of the satellite geometry effects, followed by a high-pass filtering operation to ensure that we extract fluctuations on a scale of 10 seconds or less. A third-order polynomial fit to the differenced carrier phase over a continuous interval of time can be subtracted from the differenced carrier phase to remove the satellite geometry effects. More details on the procedure of removing receiver clock effects and satellite geometry effects from the CASES carrier phase are discussed by *O'Hanlon et al.* [2011].

[17] For our scintillation studies, we are interested in high-frequency variations introduced by scintillations. Therefore,

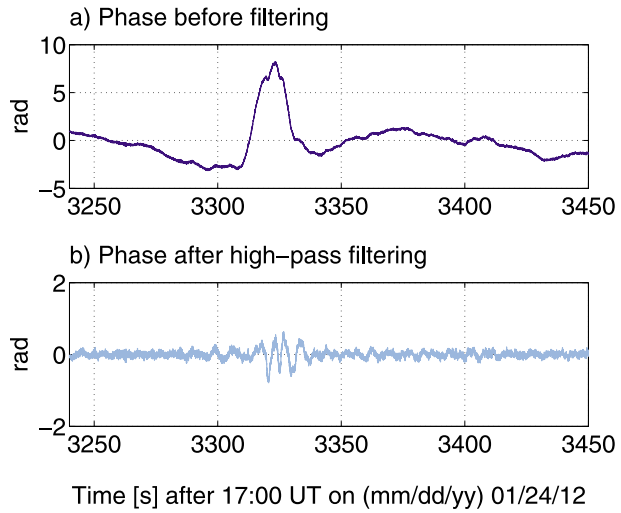

Figure 1. Phase of PRN 9 signal on 24 January 2012, System 4: (a) the phase after polynomial fit-subtraction and (b) the phase after high-pass filtering using a Butterworth filter implemented in the frequency domain.

a differenced IQ phase is added to the differenced carrier phase to obtain phase which contains frequency components up to the pre-detection bandwidth of 50 Hz. This differenced phase then undergoes polynomial fit subtraction. To obtain the final detrended phase, any residual low frequency variations are subsequently removed from the phase by using a high-pass sixth-order Butterworth filter in the frequency domain as indicated by *Van Dierendonck and Hua* [2001]. We generally use a 3-dB cut-off frequency of 0.1 Hz for the filter. In the case of data segments shorter than 60 seconds, we use a cut off frequency of 0.2 Hz. In Figure 1, we demonstrate the effectiveness of the high-pass filter to extract high frequency phase. Ionospheric scintillation data detrending is discussed in detail by *Forte and Radicella* [2002].

[18] The data analysis procedure to detrend the high-rate phase data can be summarized symbolically as follows. If $\phi_{cs}(t)$ and $\phi_{cref}(t)$ are the time series of the carrier phase on scintillating and reference channels, respectively, we obtain differenced carrier phase time series $\phi_c(t)$ as

$$\phi_c(t) = \phi_{cs}(t) - \phi_{cref}(t) \tag{1}$$

Similarly, differenced IQ phase time series $\phi_{iq}(t)$ is obtained by subtracting the IQ phase on the reference channel ($\phi_{iq_{ref}}(t)$) from the IQ phase on the scintillating channel ($\phi_{iq_s}(t)$):

$$\phi_{iq}(t) = \phi_{iq_s}(t) - \phi_{iq_{ref}}(t) \tag{2}$$

The differenced carrier and IQ phases are added together to obtain the phase $\phi(t)$ which contains frequency components up to the pre-detection bandwidth:

$$\phi(t) = \phi_c(t) + \phi_{iq}(t) \tag{3}$$

A third-order polynomial fit $\widetilde{\phi}(t)$ of the phase $\phi(t)$ is subtracted from itself to obtain phase $\phi'(t)$ with predominantly high frequency components:

$$\phi'(t) = \phi(t) - \widetilde{\phi}(t) \tag{4}$$

A high-pass filtering of phase $\phi'(t)$ removes any residual low-frequency components and produces the final filtered phase $\phi_f(t)$. This data processing procedure used to obtain the detrended high-rate CASES phase is summarized in Figure 2.

[19] To detrend the high-rate power time history, we follow the procedure described by *Van Dierendonck and Hua* [2001], where the raw power data ($I^2 + Q^2$) are high-pass filtered with a sixth-order Butterworth filter. Note that receiver clock variations do not significantly affect signal power; thus, signal differencing to remove clock errors is not required for power data. However, it should be mentioned that the detrending of power is carried out on continuous segments with times corresponding to those of the processed phase data segments. To detrend power, high-pass filtering is performed by initially generating a sixth-order low-pass

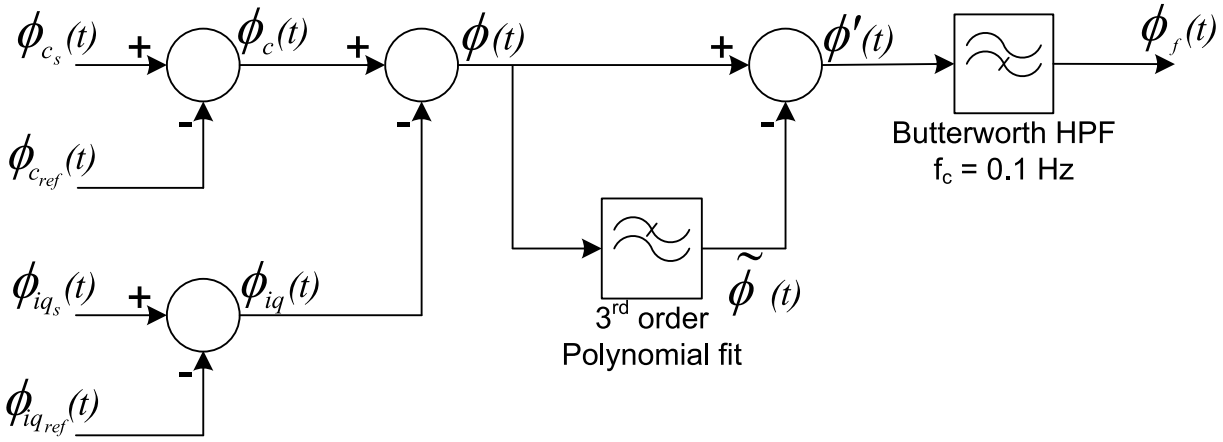

Figure 2. A block diagram summarizing the data processing procedure used to obtain the detrended phase data from the CASES receiver. HPF stands for high-pass filter.

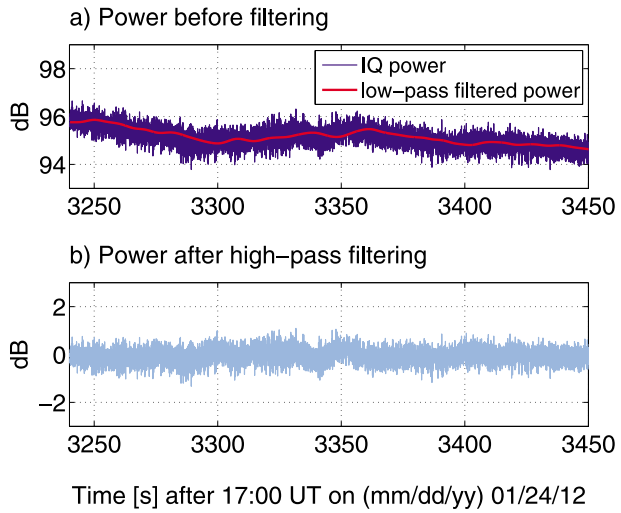

Figure 3. Power of PRN 9 signal on 24 January 2012, System 4, (a) before and (b) after high-pass filtering. High-pass filtered signal (Figure 3b) is obtained by dividing the IQ "raw" power (blue graph in Figure 3a) by low-pass filtered power (red graph in Figure 3a).

Butterworth filter with a typical 0.1 Hz cut-off, applying this filter to the power of a scintillating PRN to obtain a low-pass-filtered output, and finally dividing the original power of that PRN by the low-pass-filtered power. Therefore, if $P_r(t)$ is the data segment with a time series of the raw power, and $P_{LPF}(t)$ is the time series obtained by low-pass filtering $P_r(t)$, the high-pass filtered power $P_f(t)$ is given as

$$P_f(t) = \frac{P_r(t)}{P_{LPF}(t)} \tag{5}$$

The 0.1 Hz cut-off is flexible and can be adjusted to ensure that all low-frequency effects are removed from the data. If the continuous data segments are smaller than 60 seconds, we use a cut-off frequency of 0.2 Hz instead of 0.1 Hz, as with the phase filtering operation. The effectiveness of high-pass filtering on power, i.e. dividing out the low-pass filtered power, is seen in Figure 3.

[20] The scintillation index $S4$ is typically derived from detrended signal intensity SI which is in turn obtained by taking the square root of detrended power. $S4$ is defined as follows:

$$S4 = \sqrt{\frac{\langle SI^2 \rangle - \langle SI \rangle^2}{\langle SI \rangle^2}} \tag{6}$$

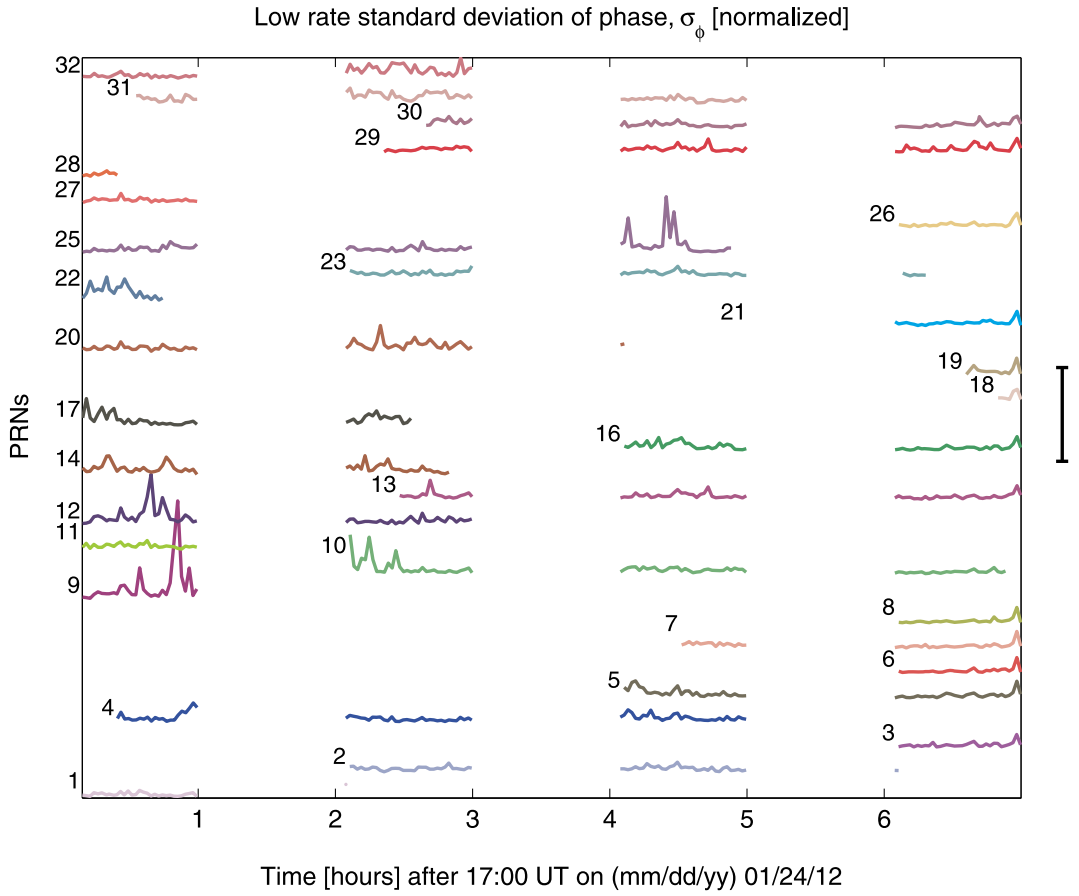

Figure 4. Stack plots from System 4 of low-rate σ_ϕ for all available PRNs. This figure shows GPS satellite availability with respect to time in UT on 24 January 2012.

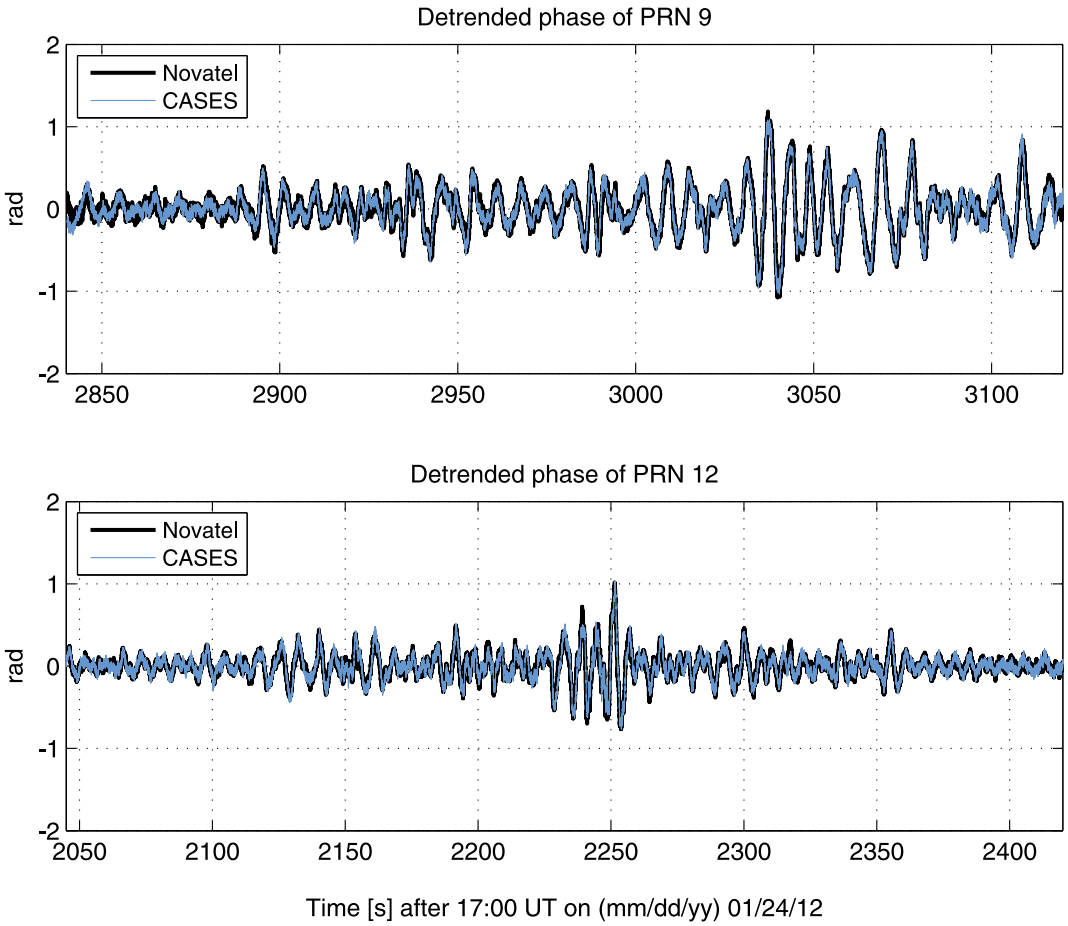

Figure 5. Plots comparing Novatel and System 4 CASES phase data on 24 January 2012 for PRN 9 and PRN 12.

where the angular bracket represents a time average, commonly taken over a 60-second interval. The standard deviation of the phase σ_ϕ is computed over the same interval. For CASES power and phase data segments longer than 60 seconds, we use a 1 minute-long sliding window for both $S4$ and σ_ϕ computations. CASES low-rate data consists of $S4$ and σ_ϕ precomputed by SCINTMON, which can be used with the high-rate scintillation parameters to determine the scintillating time periods as illustrated in the next section.

4. CASES Results and Comparison With Data from the Novatel Receiver

[21] The CASES measurements reported here were recorded from AAL-PIP System 4 (89.998°S, 124.075°E) on 24 January 2012. About 17 hours of low-rate and about 9 hours of high-rate data were collected during the CASES storm mode within the period of 24 January to 26 January 2012. The GPS receiver was switched to storm mode a little after 17:00 UT on 24 January 2012. This was to capture any interesting scintillating events possibly originated by a CME reaching the Earth from an M9-class solar flare that erupted on 23 January around 03:59 UT from sunspot 1402. The CASES receiver recorded low-rate data on 2 frequencies during these measurements, namely, GPS L1 legacy civil code (L1CA) and GPS L2 civil L code (L2CL). Useful high-rate data were detected on L1CA. Concern over high temperatures in the insulated AAL-PIP electronics enclosure limited CASES operation to a 50% duty cycle in 1-hour increments. It is expected that this limitation will be eliminated in the future as the AAL-PIP electronics prove their ability to operate at high temperatures.

[22] Stack plots of low-rate standard deviation of phase σ_ϕ for each available PRN as recorded on 24 January 2012 by System 4 CASES on the L1CA signal are shown in Figure 4. For each PRN, σ_ϕ is normalized using the maximum detected value of σ_ϕ in all the available low-rate data on that day. The horizontal axis on the plot represents time in UT, while the vertical axis displays the PRN of the available satellite. The vertical scale on the right hand side of the plot corresponds to the maximum value of phase standard deviation in the stack plot, which might occur on any of the PRNs (for this case, it is PRN 9). The stack plots reveal some interesting possible phase scintillation events, for example, on PRN 9 and PRN 12. Figure 4 can be considered as a daily summary plot as it depicts the availability of different satellites with recorded low-rate data. During the four hours of ON time on January 24, the receiver collected about 37 MB of low-rate and raw high-rate data. The high-rate data were then analyzed using the post-processing technique described in section 3. We have generated stack plot similar

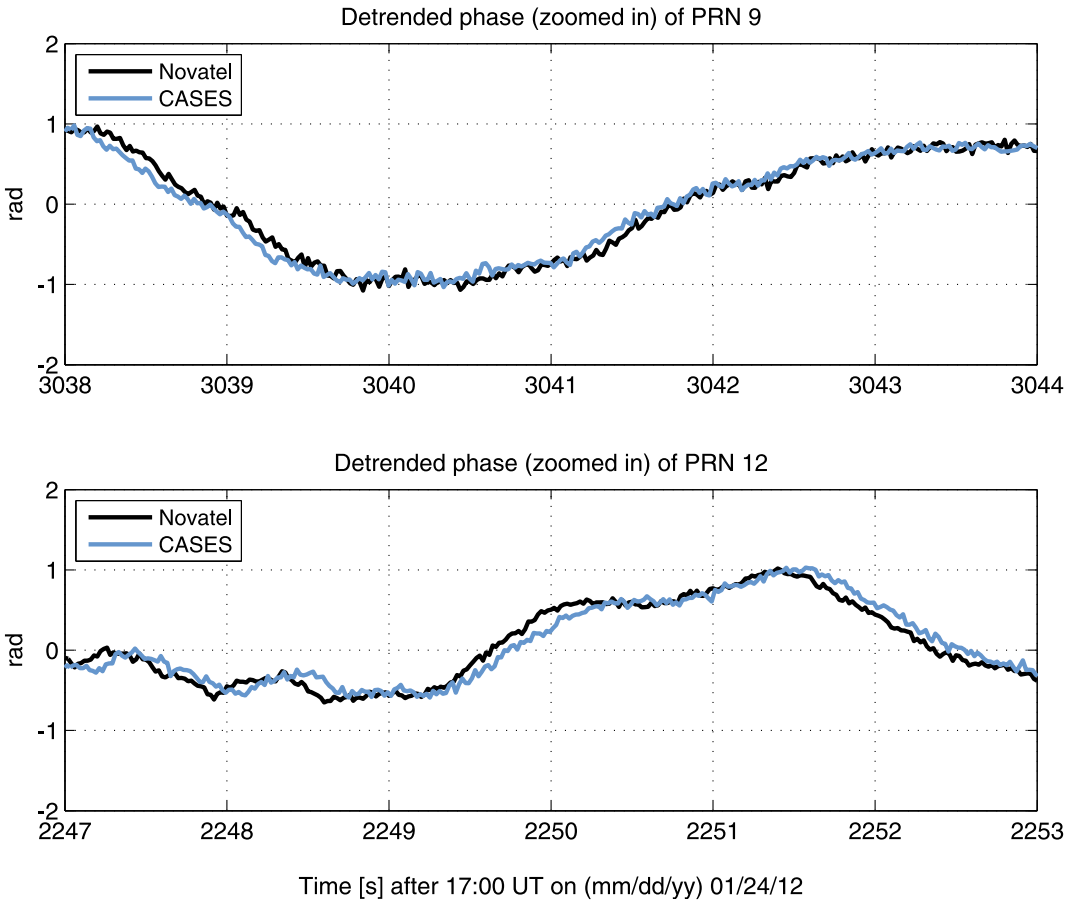

Figure 6. Plots after zooming in on Figure 5 showing the time delay between the Novatel and System 4 CASES phase data on 24 January 2012 for PRN 9 and PRN 12.

to Figure 4 with high-rate standard deviation of phase. This plot indicated the availability of different satellites with recorded high-rate data. Because of the facility of selecting and storing interesting events, the high-rate data availability covered much less total time than the low-rate data.

[23] The two events considered for study in this paper are observed using the signals from PRN 9 and PRN 12 on L1CA frequency after 17:30 UT on 24 January 2012. These events are clearly visible in Figure 4. The processed high-rate data for these events showed strong phase scintillations for a duration of about 60 seconds. The scintillations were found to have a dominant period of 6 seconds. The Novatel receiver used for comparison was about 1.5 kilometers away from the CASES GPS receiver. With such a short baseline, the scintillation data from the two receivers should be strongly correlated. In order to compare the two events with the Novatel data, the power and phase obtained from the Novatel receiver at South Pole were processed with the same techniques used for CASES. Specifically, the power was divided by the low-pass filtered power, and for the phase, a polynomial fit was subtracted followed by a high-pass Butterworth filtering operation in the frequency domain. The Novatel receiver uses an oven-controlled SC-cut crystal oscillator (OCXO), which is stable enough that clock variations do not significantly corrupt phase measurements, as discussed by *Van Dierendonck and Hua* [2001]. Therefore, no differencing operation was required for phase from the Novatel receiver.

[24] A comparison between detrended phase obtained from the CASES and Novatel receivers for the 2 PRNs is shown in Figure 5. It is evident from the plot that CASES reproduces phase as obtained from the Novatel receiver. The detrended power for the CASES and Novatel receivers also agree closely, but the power variation was observed to be less than 1 dB, indicating that these events are predominantly phase scintillations. A careful examination of phases in a shorter time duration, as shown in Figure 6, revealed that the CASES phase for PRN 9 leads the Novatel phase by 0.12 seconds. Scintillations on PRN 12 indicated that the Novatel phase leads the CASES phase by 0.12 seconds. The close agreement between the two receivers implies little to no horizontal motion of the irregularities causing scintillation.

[25] For the case of this 24 January 2012 study, a thorough comparison of the available CASES data with Novatel data showed that apart from the two scintillation events from Figure 5, all the events in CASES were confirmed detections. However, a few weak scintillation events from the Novatel receiver were not detected by the CASES receiver, presumably because they were not sufficiently strong to trigger CASES high-rate data output for the triggering threshold that was implemented at the time. To obtain good statistics of CASES performance at high latitudes, a large amount of

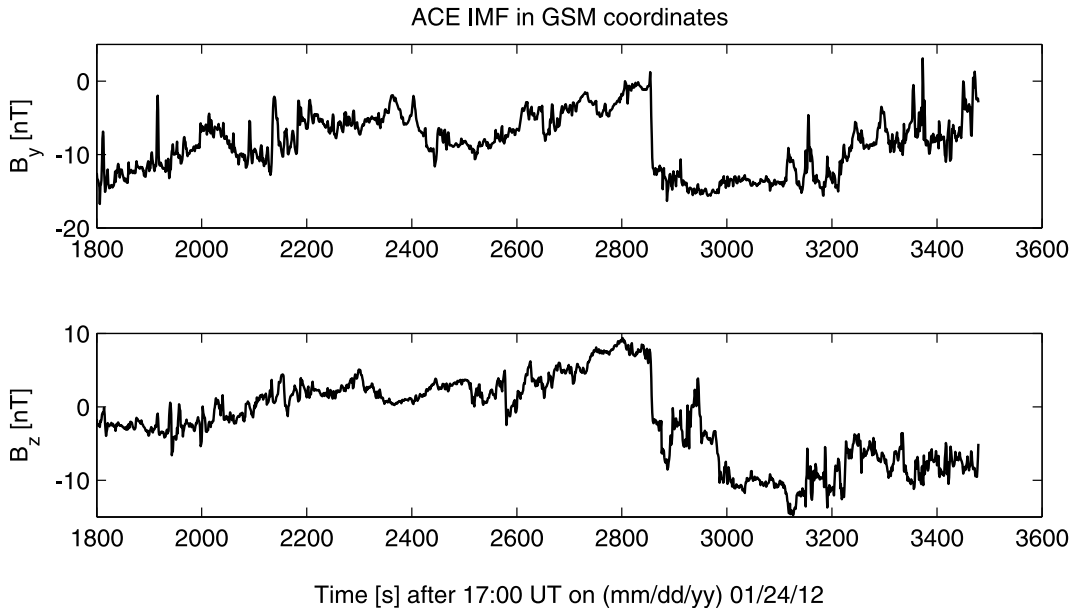

Figure 7. ACE IMF B_y and B_z components with 1 Hz sampling frequency at the ACE satellite position in geocentric solar magnetospheric (GSM) coordinates on 24 January 2012 from 17:30 UT to 18:00 UT.

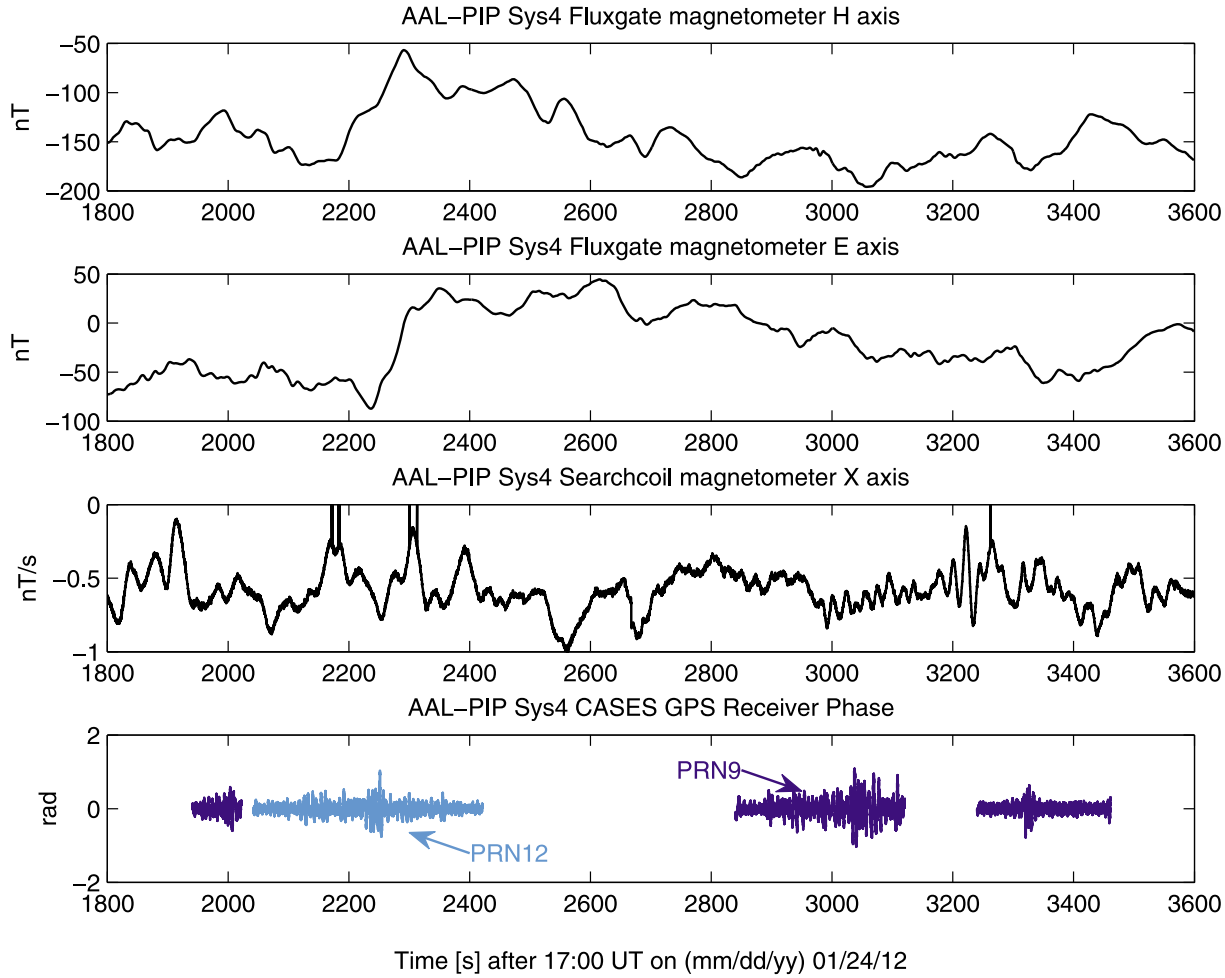

Figure 8. System 4 CASES GPS receiver phase for PRN 9 and PRN 12 plotted with observations from System 4 AAL-PIP magnetometers on 24 January 2012.

additional data needs to be collected to ensure statistical significance. We are experimenting with different storm mode strategies and different threshold values for the AAL-PIP CASES to permit collection of large data sets useful for statistical study.

[26] The interplanetary magnetic field (IMF) observations obtained from the Advanced Composition Explorer (ACE) spacecraft are plotted in Figure 7 from 17:30 UT to 18:00 UT. ACE is located close to the L1 Lagrange point, a position between the Sun and the Earth about 1.5 million km from the Earth. The solar wind data recorded during this time was 285 km/s. This implies that, at this time, the solar wind observed at ACE took about 88 minutes to arrive at the Earth. The magnetic field components in Figure 7 are in geocentric solar magnetospheric (GSM) coordinate system. Both B_y and B_z displayed sharp changes ~3000 seconds after 17:00 UT, with B_y going from ~0 nT to −15 nT and B_z going from ~+10 nT to −10 nT. These changes in B_y and B_z appear to occur at approximately the same time as the GPS phase fluctuations shown in the bottommost panel in Figure 8.

[27] Furthermore, we compared the CASES phase fluctuations with observations from the AAL-PIP fluxgate and search coil magnetometers for the same time period. Our preliminary comparison of the CASES GPS phase with observations from AAL-PIP magnetometers on System 4 is illustrated in Figure 8. The coordinate system for fluxgate magnetometer conforms to H(geomagnetic north), E(geomagnetic east) and Z(vertically down toward the center of the Earth) system. The coordinate system for search coil magnetometer is X(geomagnetic south), Y(geomagnetic west) and Z(along the field line). A cursory inspection of the plots suggests that the GPS scintillation events may be causally connected to the magnetometer observations. Comparing the plots, it appears that the GPS phase fluctuations from PRN 12 starting approximately at 2200 seconds after 17:00 UT are correlated with significant deflections in the fluxgate H and E axes, while the fluctuations on PRN 9 at ~3100 s after 17:00 UT seem to be correlated with wave-like variations in the searchcoil X axis. The possible correlations between the observed GPS phase scintillations and the changes in IMF, the deflections in the fluxgate H and E axes, and the wave-like variation in the searchcoil X axis, will be investigated in detail in a later paper.

5. Summary and Conclusions

[28] Initial results from a CASES GPS receiver deployed at high latitudes have been presented. Our experiment of deploying to the Eastern Antarctic Plateau autonomous space science platforms, AAL-PIPs, equipped with the novel CASES GPS receiver, has also been discussed. For testing purposes, three AAL-PIP systems with CASES receivers have been established at the South Pole. As part of our study, we have developed and applied specialized post-processing techniques to analyze CASES high-rate data. Results of GPS phase scintillations observed during the solar storm of 24 January 2012 have been reported. We have compared the CASES high-rate IQ data with data from a Novatel GSV4004 GPS scintillation receiver at the South Pole, and we have determined that there is a good match in phase scintillations between the two. From this study, it is clear that CASES can be reliably used as a science grade GPS scintillation detection monitor to record phase scintillations at high latitudes.

[29] For further study, scintillation events such as those from the 24 January 2012 storm can be inspected in detail using ancillary observations from other AAL-PIP instruments. Specifically, the fluxgate and search coil magnetometers suggest a connection between GPS scintillations and IMF and magnetometer observations. A detailed study examining observations from these instruments and a forward propagation model should prove useful to understanding the physics of high latitude ionospheric irregularities. Utilizing all available AAL-PIP CASES receivers at the South Pole along with the Novatel receiver for correlation scintillation studies should also be explored.

[30] When the AAL-PIP stations are deployed to their final destinations along the 40° magnetic meridian and are each separated by a couple hundred kilometers from the nearest adjacent station, AAL-PIP CASES scintillation results may yield information about possibly drifting irregularities. This will facilitate comparison of occurrence of scintillations in the auroral, polar cap, and cusp regions. We will then be able to compare these observations with those from GPS receivers in the northern high latitudes to investigate whether simultaneous scintillations occur in the conjugate auroral regions.

[31] **Acknowledgments.** We would like to thank the National Science Foundation for supporting this research under grants ANT-0839858, ATM-922979 and ANT-0840650. We are grateful to Cathryn Mitchell and Joe Kinrade of University of Bath, UK for sharing the South Pole Novatel GPS data with us.

References

Aarons, J. (1982), Global morphology of ionospheric scintillations, *Proc. IEEE*, *70*(4), 360–378, doi:10.1109/PROC.1982.12314.

Akos, D. M., P.-L. Normark, P. Enge, A. Hansson, and A. Rosenlind (2001), Real-Time GPS Software Radio Receiver, in *Proceedings of the 2001 National Technical Meeting of the Institute of Navigation*, pp. 809–816, Inst. of Nav., Manassas,Va.

Basu, S., E. J. Weber, T. W. Bullett, M. J. Keskinen, E. MacKenzie, P. Doherty, R. Sheehan, H. Kuenzler, P. Ning, and J. Bongiolatti (1998), Characteristics of plasma structuring in the cusp/cleft region at Svalbard, *Radio Sci.*, *33*(6), 1885–1899, doi:10.1029/98RS01597.

Basu, S., K. M. Groves, Su. Basu, and P. J. Sultan (2002), Specification and forecasting of scintillations in communication/navigation links: current status, and future plans, *J. Atmos. Sol. Terr. Phys.*, *64*(16), 1745–1754, doi:10.1016/S1364-6826(02)00124-4.

Beach, T. L. (1982), Global Positioning System studies of equatorial scintillations, PhD thesis, Cornell University, Ithaca, N. Y.

Coster, A., S. Skone, C. Mitchell, G. De Franceschi, L. Alfonso, and V. Romano (2005), Global studies of GPS scintillation, in *Proceedings of the 2005 National Technical Meeting of the Institute of Navigation*, pp. 1130–1139, Inst. of Nav., Manassas, Va.

Crowley, G., G. S. Bust, A. Reynolds, I. Azeem, R. Wilder, B. W. O'Hanlon, M. L. Psiaki, S. Powell, T. E. Humphreys, and J. A. Bhatti (2011), CASES: A novel low-cost ground-based dual-frequency GPS software receiver and space weather monitor, in *Proceedings of the 24th International Technical Meeting of the Satellite Division of the Institute of Navigation*, pp. 1437–1446, Inst. of Nav., Manassas, Va.

Forte, B., and S. M. Radicella (2002), Problems in data treatment for ionospheric scintillation measurements, *Radio Sci.*, *37*(6), 1096, doi:10.1029/2001RS002508.

Ganguly, S., A. Jovancevic, A. Brown, M. Kirchner, S. Zigic, T. Beach, and K. Groves (2004), Ionospheric scintillation monitoring and mitigation using a software GPS receiver, *Radio Sci.*, *39*, RS1S21, doi:10.1029/2002RS002812.

Kinrade, J., C. N. Mitchell, P. Yin, N. Smith, M. J. Jarvis, D. J. Maxfield, M. C. Rose, G. S. Bust, and A. T. Weatherwax (2012), Ionospheric scintillation over Antarctica during the storm of 5–6 April 2010, *J. Geophys. Res.*, *117*, A05304, doi:10.1029/2011JA017073.

Mitchell, C. N., L. Alfonsi, G. De Franceschi, M. Lester, V. Romano, and A. W. Wernik (2005), GPS TEC and scintillation measurements from the polar ionosphere during the October 2003 storm, *Geophys. Res. Lett.*, *32*, L12S03, doi:10.1029/2004GL021644.

Musko, S. B., C. R. Clauer, A. J. Ridley, and K. L. Arnett (2009), Autonomous low-power magnetic data collection platform to enable remote high latitude array deployment, *Rev. Sci. Instrum.*, *80*(4), 044501, doi:10.1063/1.3108527.

Ngwira, C. M., L. McKinnell, and P. J. Cilliers (2010), GPS phase scintillation observed over a high-latitude Antarctic station during solar minimum, *J. Atmos. Sol. Terr. Phys.*, *72*(9–10), 718–725, doi:10.1016/j.jastp.2010.03.014.

O'Hanlon, B. W., M. L. Psiaki, S. Powell, J. A. Bhatti, T. E. Humphreys, G. Crowley, and G. S. Bust (2011), CASES: A smart, compact GPS software receiver for space weather monitoring, in *Proceedings of the 24th International Technical Meeting of the Satellite Division of the Institute of Navigation*, pp. 2745–2753, Inst. of Nav., Manassas, Va.

Prikryl, P., P. T. Jayachandran, S. C. Mushini, D. Pokhotelov, J. W. MacDougall, E. Donovan, E. Spanswick, and J. P. St. Maurice (2010), GPS TEC, scintillation and cycle slips observed at high latitudes during solar minimum, *Ann. Geophys.*, *28*(6), 1307–1316, doi:10.5194/angeo-28-1307-2010.

Prikryl, P., et al. (2011), Interhemispheric comparison of GPS phase scintillation at high latitudes during the magnetic-cloud-induced geomagnetic storm of 5–7 April 2010, *Ann. Geophys.*, *29*(12), 2287–2304, doi:10.5194/angeo-29-2287-2011.

Skone, S., and K. Knudsen (2000), Impact of ionospheric scintillations on SBAS performance, in *Proceedings of the 13th International Technical Meeting of the Satellite Division of the Institute of Navigation*, pp. 284–293, Inst. of Nav., Manassas, Va.

Skone, S., G. Lachapelle, D. Yao, W. Yu, and R. Watson (2005), Investigating the impact of ionospheric scintillation using a GPS software receiver, in *Proceedings of the 18th International Technical Meeting of the Satellite Division of the Institute of Navigation*, pp. 1126–1137, Inst. of Nav., Manassas, Va.

Smith, A. M., C. N. Mitchell, R. J. Watson, R. W. Meggs, P. M. Kintner, K. Kauristie, and F. Honary (2008), GPS scintillation in the high arctic associated with an auroral arc, *Space Weather*, *6*, S03D01, doi:10.1029/2007SW000349.

Spogli, L., L. Alfonsi, G. De Franceschi, V. Romano, M. H. O. Aquino, and A. Dodson (2009), Climatology of GPS ionospheric scintillations over high and mid-latitude European regions, *Ann. Geophys.*, *27*(9), 3429–3437, doi:10.5194/angeo-27-3429-2009.

Van Dierendonck, A. J., and Q. Hua (2001), Measuring ionospheric scintillation effects from GPS signals, in *Proceedings of the 57th Annual Meeting of the Institute of Navigation*, pp. 391–396, Inst. of Nav., Manassas, Va.

Van Dierendonck, A. J., J. Klobuchar, and Q. Hua (1993), Ionospheric scintillation monitoring using commercial single frequency C/A code receivers, in *Proceedings of the 6th International Technical Meeting of the Satellite Division of the Institute of Navigation*, pp. 1333–1342, Inst. of Nav., Manassas, Va.

Wernik, A. W., J. A. Secan, and E. J. Fremouw (2003), Ionospheric irregularities and scintillation, *Adv. Space Res.*, *31*(4), 971–981, doi:10.1016/S0273-1177(02)00795-0.